Quantifying Microelectronics Reliability Under Cumulative Radiation Damage: Stress-Strength Inference with Type-I Censored Data for Failure Probability Estimation

By

Chloe Alexandra Champagne

Thesis

Submitted to the Faculty of the

Graduate School of Vanderbilt University

in partial fulfillment of the requirements

for the degree of

MASTER OF SCIENCE

in

Electrical Engineering

May 10th, 2024

Nashville, Tennessee

Approved:

Brian Sierawski, Ph.D.

Daniel Fleetwood, Ph.D.

TABLE OF CONTENTS

ACKNOWLEDGEMENTS

I would like to thank my advisor, Dr. Brian Sierawski, for his guidance and support in this research and in the graduate school journey. Thanks also to Dr. Raymond Ladbury and Michael Campola for their insights and suggestions regarding statistics and hardness assurance practices. Thanks to Dr. Daniel Fleetwood for guidance on mechanisms and testing considerations. Thank you to all the professors and students in the Radiation Effects and Reliability group, the Institute for Space and Defense Electronics, and the Scalable Asymmetric Lifecycle Engagement (SCALE) Program for introducing me to the field of radiation effects engineering. Thank you to my family and friends for their encouragement and support. Finally, thank you to the NASA Electronic Parts and Packaging (NEPP) Program for funding this work under grant no. 80NSSC23K0512.

LIST OF TABLES

LIST OF FIGURES

CHAPTER I

INTRODUCTION

Microelectronics are used in virtually every human-produced system in the modern era, making microelectronics reliability a paramount issue for engineers. As electronic parts are used, wear-down due to operational and external stresses results in degradation and eventually failure in these parts. The ability to precisely define the failure behavior of electronic parts and predict when they might fail is essential for insuring mission success. In space, the situation is even more dire than that on the surface of Earth as parts cannot be replaced, and the operational environment is far more hostile due to extreme temperature and radiation.

Radiation hardness assurance (RHA) is necessary for evaluating the suitability of an electronic part for operating in a radiation environment, particularly a space environment. Military guidelines incorporate worst-case (WC) constants for environment radiation dose and a mean part failure dose when calculating a radiation design margin (RDM) to categorize the hardness of parts for space missions [1]. However, the RDM method does not account for the variability of the environment, and categorizations lack formal mathematical rigor and design flexibility. As such, a high degree of overdesign is inherent in this method of RHA. In space missions with billion-dollar payloads and human life onboard, the overdesign required by this framework is acceptable due to the high cost of failure. However, for missions with higher risk tolerance, such overdesign may be an unnecessary burden and even prohibit mission completion. Incorporating all aspects of failure variability allows more flexibility in determining the suitability of the part for a mission. Additional engineering flexibility reduces overdesign, a cost- and time-saver that can significantly benefit NewSpace and smaller space missions (e.g., CubeSats) [2], [3].

RHA has evolved over the past decade as probabilistic radiation environment models have been released [4], [5], [6], [7]. With the availability of these probabilistic environment models, a new method to RHA was developed in [2] for analyses of total ionizing dose (TID) and displacement damage dose (DDD) effects. This method uses stress-strength inference, integrating the product of an environment dose distribution and a distribution describing device behavior over a range of doses to obtain a TID failure probability. This method is more mathematically rigorous than the RDM method and provides engineers with a metric directly incorporating the variability of both the environment and the device response separately. Using the probabilistic method allots greater design flexibility to the radiation effects engineer for qualifying the part for space usage [2].

To bound the error from device sample size, a method was developed in [3] that uses likelihood ratios to achieve a confidence-bounded family of curves and assess the worst-case failure probability. Within a 90% confidence level (CL) contour of the lognormal parameter space, the worst-case fit was selected as g(x) and used in the integration. The confidence bounds relied on fitting a set of total-dose failure levels obtained in radiation testing of the device.

This work expands the likelihood ratio method of bounding failure probability [3] to incorporate datasets consisting of devices that survived radiation testing (survivors) or a mixture of failures and survivors. This scenario occurs often in missions using commercial-off-the-shelf (COTS) technologies, as manufacturers frequently test to a certain dose rather than to failure. COTS technologies may be preferential over their radiation-hardened counterparts due to their superior performance and capacity. Therefore, developing a framework to incorporate available TID data on these parts is beneficial. To use survivor data, an alternative likelihood definition incorporating tests not followed to failure is used to identify an area of interest within the device

failure parameter space. The 90% confidence bound is used as a mask that, coupled with an upper bound on physically relevant distributions, allows for the determination of the worst-case failure probability to a 90% confidence level in a given environment with stress-strength analysis. This probability is selected as the metric for determining whether a part is suitable for use in the space environment under consideration. It is demonstrated that bounding the failure probability due to cumulative damage of piece-parts with survivor data permits a more comprehensive analysis of survivability in variable space environments than existing methods.

Some of the preceding paragraphs are reprinted and modified from C. Champagne et al., "A confidence-based approach to including survivors in a probabilistic TID failure assessment," IEEE Trans. Nucl. Sci., Early Access, Nov. 2023.

CHAPTER II

BACKGROUND ON RADIATION EFFECTS AND ENVIRONMENTS

Total Ionizing Dose (TID)

TID is a measure of the amount of ionizing energy deposited in a material per unit mass and can cause shifts in device parameters, posing a concern for devices operating in radiation environments. The parameter shifts are caused by charge build-up in gate and field oxides. As ionizing particles traverse a device, electron-hole pairs are excited out of their resting states. While electrons are swept away by electric fields, holes have much lower mobility and traverse the oxides more slowly. The holes may eventually be trapped within an oxide defect and become oxide trap charge. Additionally, holes may perturb hydrogen ions in the oxide, causing them to drift to the interface and create interface traps. This process for an MOS device is shown in Figure 1, taken from [8]. Different types of radiation generate different charge carrier yields, with Co-60 gamma rays typically having the highest yield; thus, Co-60 is often used in TID testing to generate a worst-case bound on device response. The trapped charge can deplete the substrate at the oxide interface, causing leakage paths to form in the device. Additionally, interface traps can degrade carrier mobility.

Factors contributing to TID-induced failure vary based on the type of device, device operating conditions, and radiation particle species. The very definition of failure may differ depending on the application. However, for most TID-induced parametric failure, the gradual build-up of charge in oxide regions as described above is the underlying failure mechanism. For MOS devices, the threshold voltage will shift, eventually going out of spec. Table I gives a summary of the main effects of the threshold voltage shift in MOS devices [9]. For bipolar devices, gain degradation is typically the parameter of interest [8], [10].

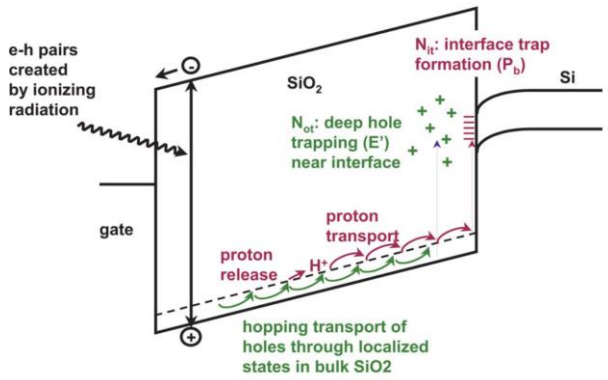

Fig. 1. Band diagram of an MOS device being irradiated, generating charge carriers in the oxide and subsequently trapping them in defects, from [8].

Table I. Device-level TID effects in MOS devices and corresponding circuit-level effects [9].

Device-Level Effect	**Circuit-Level Effect**
+/- ΔV_{TH} NMOS, - ΔV_{TH} PMOS	Failure to switch
- ΔV_{TH} NMOS	Excessive leakage current
+ ΔV_{TH} NMOS, - ΔV_{TH} PMOS	Speed reduction
+/- ΔV_{TH} NMOS, - ΔV_{TH} PMOS	Loss of noise immunity

Displacement Damage (DD)

DD occurs when incident energetic particles displace atoms within the lattice of a material. The displaced atom and corresponding gap in the atomic lattice form a 'Frenkel pair', and the stability of the pair is determined by dopants and impurities in the atomic lattice. A single displaced atom is known as a point defect, while larger cascades of defects are called cluster defects. Certain types of radiation, like gamma rays and electrons, tend to produce point defects, while neutrons tend to generate cluster defects. Energy ranges for protons and primary knock-on atoms and the corresponding defects are shown in Fig. 2. Cluster defects are more stable than point defects and

take longer to anneal. As such, neutrons tend to produce a worst-case bound on displacement damage effects [11].

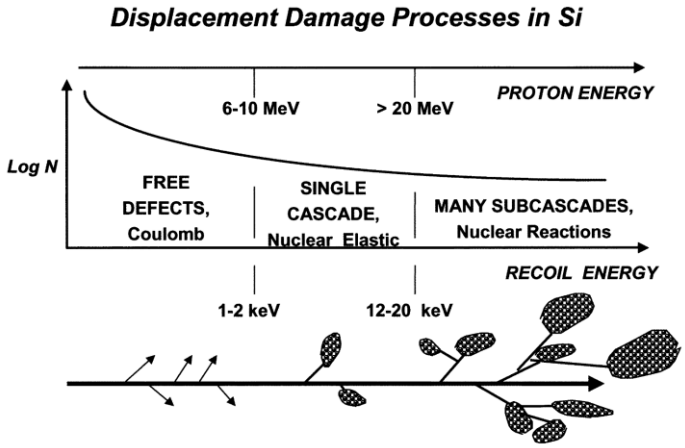

Fig. 2. Number of defects (N) as a function of incident particle energy, with a corresponding schematic of displacement damage defects. Taken from [11].

Like with TID, DD can produce a variety of effects in devices which degrade performance and ultimately lead to parametric failure. The primary mechanism is the introduction of extra states in the band gap of the semiconductor, reducing the lifetime and mobility of minority carriers and enabling tunneling through energy barriers, as seen in Fig. 3. This can result in gain degradation in bipolar transistors as recombination current in the base-emitter junction increases, power output degradation in LEDs, and charge transfer ratio degradation in optocouplers [11], [12], [13], [14].

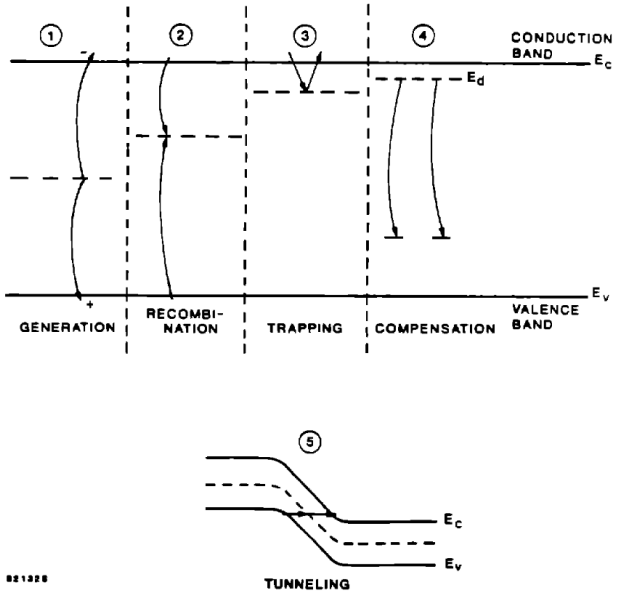

Fig. 3. Five device-level effects resulting from extra band gap states induced by displacement damage. Taken from [12].

The amount of damage induced by DD can be measured with displacement damage dose (DDD), an equivalent to rads for TID. DDD is calculated with the following equation,

$$DDD = C \times NIEL \times \varphi \tag{1}$$

where NIEL is the non-ionizing energy loss parameter, φ is the incident fluence, and C is a unit conversion constant. If C is 1, then DDD is in units of MeV/g [2]. Additionally, for a spectrum of fluence, DDD is calculated with the following,

$$DDD = \int NIEL(E) \cdot \frac{d\varphi}{dE} dE \tag{2}$$

where E is the energy of the incident particle [13]. NIEL allows incident fluence to be correlated with device damage and is the standard for DD hardness assurance, although it does have significant limitations [11].

Variability of Part TID and DD Response

In the field of reliability, cumulative, parametric failure is often described with the lognormal distribution [15], [16], [17]. The underlying reason for this behavior is that the failure mechanism can often be described by the multiplication of random variables [17], [18]. This scenario is also seen in TID and DD degradation and can be used to justify the usage of a lognormal distribution to model these failure modes.

Eq. 3 shows the TID-induced hole yield after initial recombination for the oxide of an irradiated device. N_h is the hole yield, $f(E_{ox})$ is a yield factor as a function of the electric field across the oxide, g_o is the initial charge pair density per rad (material dependent), D is the total dose in rads, and t_{ox} is the oxide thickness [8].

$$N_h = f(E_{ox}) g_o D t_{ox} \tag{3}$$

Many of the terms in this equation are random variables. For instance, g_o and t_o will vary part-to-part due to process and wafer variation. $f(E_{ox})$ will also be affected by variation in the incident radiation and the production of free charge carriers as the device is being irradiated. As such, the hole yield is the product of random variables. Additionally, the parameter g_o is on the order of 10^{12}-10^{13} pairs/cm^3/rad (for SiO_2), so as devices are irradiated well into the kilorads, charge carriers are multiplied heavily within the oxide.

The holes will either be annealed out of the oxide (e.g., neutralized by tunneling electrons, thermal emission) [19] or become trapped within defects in the oxide or at the oxide/substrate interface. Additionally, some holes may perturb the oxide lattice as they transport through, dislodging hydrogen ion impurities. Those that become trapped in the oxide form a trap density N_{ot}, while the traps at the interface (likely a result of the hydrogen ions) form the trap density N_{it}. The threshold voltage shift induced in a part may then be calculated as in (4). The individual

voltage shifts in MOS devices due to oxide and interface traps, along with the net threshold voltage shift, are shown in Figure 4, taken from [20]. The multiplicative nature of hole formation and of underlying variation in this process between devices is what causes TID-induced parametric failure to follow a lognormal distribution across different device types.

$$\Delta V_{th} = q\Delta N_{it}/C_{ox} + q\Delta N_{ot}/C_{ox} \tag{4}$$

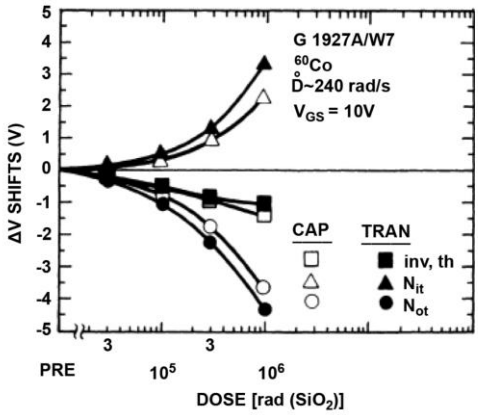

Fig. 4. Voltage shifts in capacitors and transistors due to oxide traps and interface traps, and total inversion/threshold shift, as functions of dose. Taken from [20].

Failure due to DDD can be modelled with the lognormal distribution as well [2], with similar justification. NIEL, one of the primary components of DDD, is the energy loss due to elastic and nuclear inelastic collisions and is correlated with a device's damage factor, or the amount of device degradation of a particular parameter. It is calculated with the following,

$$NIEL = \left(\frac{N}{A}\right)[\sigma_e T_e + \sigma_i T_i] \tag{5}$$

where N is Avogadro's number, A is the gram atomic weight of the material, σ_e and σ_i are the elastic and inelastic cross sections, and T_e and T_i are the effective average recoil energies (corrected for ionization loss) from the elastic and inelastic collisions [11]. Both σ's and T's are random variables

which vary from device to device, as well as the radiation particle fluence in (1). As such, DDD results from the multiplication of random variables and can be modelled with the lognormal distribution.

The part variability discussed in this section is particularly problematic with COTS parts. In general, parts from different lots may exhibit systematically different failure behavior due to processing changes, both purposeful and inadvertent. This problem is amplified with COTS parts, as the process may not be regulated and may be changed without warning [21], [22]. Additionally, the wafer or production lot information for COTS parts may not be available or made public, so the very definition of a COTS "lot" becomes ambiguous [21]. A COTS "lot" may simply consist of all parts bought in a single purchase.

Even within a single wafer, variations in doping, layer thicknesses, and other properties across the wafer result in radiation response variation, affecting RHA practices [23], [24], [25], [26]. Using small sample sizes to derive the parameters of this distribution may yield substantial errors even when testing controlled devices. In the case of COTS parts, where the wafer location of a given part is unlikely to be known, it is not possible to know if the sample will encompass the full range of the lot failure distribution.

The harness assurance framework discussed in this thesis accounts for the part performance uncertainty in a mathematically rigorous way, as detailed in the following chapter. This work does not attempt to account for lot-to-lot variability, in which multi-modal distributions may appear.

Probabilistic Environment Models

The previous standard models for the trapped particle environment in Earth's magnetosphere were AE8 and AP8. These models provided deterministic, omnidirectional electron

and proton fluxes, respectively, based on more than 20 satellite data sources from the 1960s and 1970s. Versions for solar maximum and solar minimum exist; there are no means for interpolating to intermediate points in the solar cycle. Additionally, AP8 models have their most uncertainty at low-altitude orbits [27], [28].

These models have been the de facto standard for modelling the near-Earth radiation environment due to the range of particle energies and radiation belt coverage. Electrons in the range of 0.04 MeV-7 MeV and protons in the range of 0.1 MeV-400 MeV are covered. However, extrapolation is used to cover some of this range (e.g., arbitrary power law used for <1 MeV). Additionally, the models are static, meaning that they do not encompass the dynamic nature of the radiation belts (and, strictly speaking, are only valid for the time periods the data was obtained) [28].

The AE9 and AP9 models incorporate new radiation data from 45 satellite sources and produce statistics which incorporate both the measurement and space weather uncertainty. Confidence intervals are calculated to support system designs at various degrees of criticality [29].

In terms of coverage, the AE9 covers electrons in the range of 0.04 MeV-10 MeV, a slight improvement from AE8. Additionally, for total dose calculations, bremsstrahlung is included in the output. For AP9, proton coverage in the range of 0.1 MeV-2 GeV provides a much larger range than the AP8 predecessor. Data from a wide range of the solar cycle, not just the solar max and min, are used in the models [4].

Flux maps are derived from satellite data using the median and 95th percentile of the fitted distribution function. Error maps accounting for instrument uncertainties are also produced. Interpolation algorithms are applied to fill the space between satellite measurements. A Monte Carlo model is used to compute a spatiotemporal covariance matrix to account for space weather

dynamics. By running the model N times with different random seeds, the user can get N different flux profiles and compute desired statistics with the sample profiles [4].

The model can be run in three modes: mean, perturbed mean, and Monte Carlo. The mean mode acts much like the AP8/AE8 models and only utilizes the mean flux maps. The perturbed mean mode includes uncertainty from measurements and data gap extrapolations with the flux map. The Monte Carlo mode is similar to the perturbed mean mode with the addition of space weather variability [4].

Users can interact with the model through a command line interface or a GUI interface. The user must input either orbital parameters or an ephemeris file, as well as which statistics to compute. Output text files populate the set output directory, and this data can be used to plot flux, fluence, and total dose curves. Users can run in mean, perturbed mean, and Monte Carlo modes. The software can be downloaded for Windows on the Air Force Research Laboratory's website [30].

The ESP model, implemented by NASA, incorporates data from the past three solar cycles to fit a distribution of proton fluences during solar maximum at a distance of 1 AU from the Sun. Other solar proton models, such as the King and JPL models, only incorporate solar cycle 19 and 20 and are limited in the number of data points used, therefore limiting their statistical validity (King more so than JPL). Additionally, these models were largely empirical, and the data fit to either a lognormal distribution or a power law distribution. These fits, however, poorly estimated the extremes of the fluence distribution (the largest and smallest events) [5].

One of the key advantages of the ESP model is that the selection of the underlying distribution is based on Maximum Entropy Theory – the number of event fluences are fit to a truncated power law selected in such a way as to minimize the bias of a fit. From this initial

distribution, model parameters for a lognormal distribution predicting the total fluence over a desired number of solar active years is found. Not only does this method result in a more accurate data fit, but it also adds mathematical rigor to the process of selecting a fit. Moreover, data from solar cycles 20-22 are used, incorporating more data points than previous models and expanding the proton energy range covered [5].

The following equations are used to calculate the lognormal parameters for the total differential fluence in a single solar active year 1 AU from the Sun,

$$\Phi_{mean} = exp\left(\mu + \frac{\sigma^2}{2}\right) \tag{6}$$

$$\Phi_{RV} = \exp(\sigma^2) - 1 \tag{7}$$

where Φ_{mean} is the mean fluence, Φ_{RV} is the relative variance of the fluence, and μ and σ are the lognormal distribution parameters describing the cumulative fluence over the solar active year. The Φ_{mean} can be multiplied by T and Φ_{RV} divided by T to adjust the cumulative fluence distribution parameters for T active years [5].

ESP is implemented in a software package distributed by NASA and can be requested for Windows machines [31]. It is also available on SPENVIS [32].

To use these models with the probabilistic framework, Monte Carlo simulations were performed in order to generate cumulative distribution functions (CDFs) describing the probability of encountering a certain amount of TID or DD over the course of a mission in a particular orbit. Each trial was ranked from smallest to largest, and the percentile of each trial was found by dividing the rank by the number of trials plus one.

CHAPTER III

PROBABILISTIC HARDNESS ASSURANCE FRAMEWORK

Stress-Strength Analysis in Reliability

While stress-strength analysis is often associated with materials science, many other fields, including microelectronics reliability, must consider the "stresses" and "strengths" specific to their components and systems. Microelectronics engineers may not have to deal with failure due to physical wear and friction, but other stressors, such as electric fields, heat, and radiation, may result in failure if a part's tolerance, or "strength", is surpassed [33], [34], [35].

As derived in [34] and [35], when the stress and strength of a part can be described probabilistically, the probability of the part's failure when exposed to the stressor can be written as,

$$P(s > g) = \int_{x=0}^{\infty} \big(1 - F_s(x)\big) f_g(x) dx \tag{8}$$

where s is the stress on the part, g is the strength of the part, $F_s(x)$ is the cumulative distribution function (CDF) of the stress, and $f_g(x)$ is the probability density function (PDF) of the strength. The following sections will demonstrate how this formulation can be applied to microelectronics vulnerable to TID and DDD.

The following paragraphs and figures are reprinted and modified from C. Champagne et al., "A confidence-based approach to including survivors in a probabilistic TID failure assessment," IEEE Trans. Nucl. Sci., Early Access, Nov. 2023.

Accounting for Environment Variability

Eq. 9 is used to calculate a failure probability for a device vulnerable to TID or DDD in a radiation environment, where x is the total dose, $H(x)$ is the environment dose CDF, $g(x)$ is the device failure dose probability density function (PDF), and P_{fail} is the failure probability [2].

$$P_{fail} = \int [1 - H(x)] \cdot g(x) dx \tag{9}$$

To create the TID environment dose distribution, the AP9, AE9, and ESP models are used to generate Monte Carlo runs of 1-year geosynchronous earth orbit (GEO) doses. SHIELDOSE2 was used to transport the dose through 200 mils of Al shielding. Trials were ordered by dose to generate a CDF of the total dose distribution for the environment. To achieve a 2-year environment, doses were multiplied by 2, shown in Fig. 5. This serves as $H(x)$ in (9).

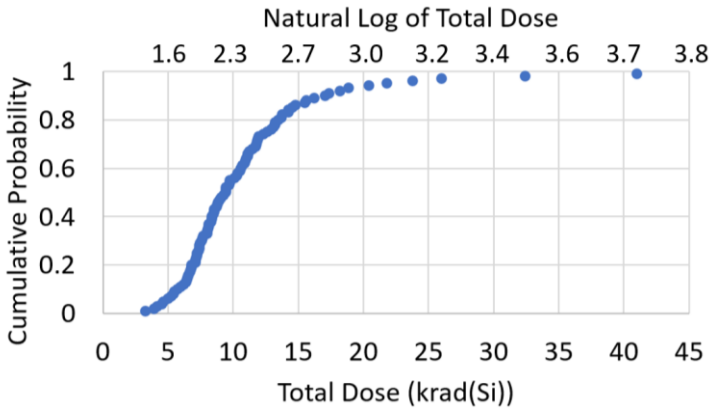

Fig. 5. The distribution H(x) of environmental doses for a 2-year GEO orbit with 200 mils of Al shielding. Doses were generated for a 1-year mission with AP9, AE9, and ESP Monte Carlo trials, ranked, and multiplied by 2.

Displacement damage dose CDFs follow a similar routine. However, because SHIELDOSE-2 only generates TID as output, another shield transport code needed to be used to get transported flux values for the DDD calculation. This will be discussed in detail in Chapter IV.

The device failure PDF *g(x)* is generated by fitting failure data found in ground-based radiation testing of the device to a lognormal distribution.

Accounting for Error in *g(x)*

Due to severe time and budget constraints, the sample sizes of devices used in these tests are often small, so the uncertainty for choosing a *g(x)* to fit failure data can be quite large. Examining a family of lognormal *g(x)* curves within a desired confidence level and selecting the worst-case fit that maximizes the failure probability provides some margin against this uncertainty. A method was developed in [3] that uses likelihood ratios to achieve a confidence-bounded family of curves and assess the worst-case failure probability.

The likelihood value of a fit describes the probability that the chosen fit will produce the data in question [36]. One method for bounding fit parameters to a certain confidence level is to use likelihood ratios to create confidence contours. This method is desirable for determining confidence as it is independent of the distributions involved, so this approach may be followed regardless of assumed device failure distribution [3], [36].

As described in [3], (10) can be used to define confidence contours in the parameter space,

$$\frac{\Lambda(\{\vec{x}\},CL)}{\Lambda(\{\vec{x}\},MAX)} \sim \exp\left(-0.5 * INV\chi^2(1-CL, DOF)\right). \quad (10)$$

Here the Λ functions are the likelihood functions of a parameter set $\{\vec{x}\}$ at a desired confidence level (*CL*) and at maximum likelihood (*MAX*), and *DOF* represent the degrees of freedom of the distribution of $\{\vec{x}\}$.

With the lognormal distribution, which has two degrees of freedom, any parameter pair producing a likelihood within a factor of 10 of the maximum likelihood is within the 90% confidence contour. The parameters μ_g and σ_g are the lognormal mean and standard deviation,

respectively, and are the parameters of interest. Fig. 6 shows an example of confidence contours for lognormal fits to four failure doses of a 2N2222 transistor (taken from [3]) with the 90% confidence boundary shown by the dashed oval. Within a 90% confidence level (CL) contour of the lognormal parameter space, the worst-case fit is selected as *g(x)* and used in the integration in (9).

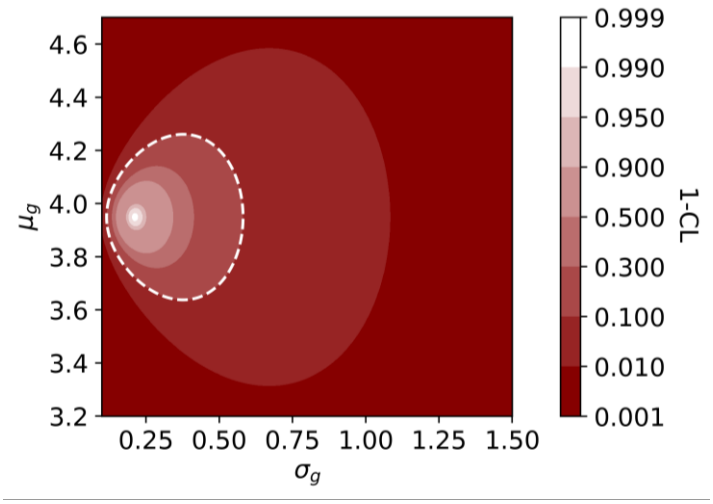

Fig. 6. A heatmap of confidence contours for lognormal fits of the following 2N2222 failure doses, in krad(Si): 39.1, 47.98, 55.18, 70. The parameter pairs with likelihood ratios >0.1 are within a 90% confidence contour (dashed oval). Reproduced from [3].

Accounting for Survivor Data

The confidence bounds thus far have relied on fitting a set of total-dose failure levels obtained in radiation testing of the device. The maximum likelihood for failure distribution parameters requires failure data, but survivor data can still be used to exclude unlikely regions of the parameter space.

To incorporate survivor data, the formulation for type-I censored likelihood is used. Failure datasets that contain survivors are known as type-I censored data. NIST provides the following definition of type-I censored likelihood [37],

$$\Lambda = C\left(\prod_{i=1}^{r} f(t_i)\right)[1 - F(T)]^{n-r} \ . \tag{11}$$

F and *f* are the CDF and PDF of the device failure distribution, respectively, t_i is the i^{th} failure dose, and *T* is the dose to which the survivors were tested. *C* is a constant that divides out and plays no part in the analysis. The product of the $f(t_i)$ values represents the likelihood of the distribution generating the *r* failure data alone. This term is multiplied by the probability of *n-r* devices surviving, generating an overall likelihood of the chosen fit reproducing the recorded data. This definition is used to generate confidence contours for device failure fits of survivor or mixed failure-survivor datasets.

Fig. 7 shows heatmaps of the type-I censored confidence contours for the parameter space of the lognormal device failure distribution, with different sized survivor datasets, tested to 40 krad(Si). The 90% confidence contour consists of regions with a likelihood ratio > 0.1 (above the dashed line). Increasing the number of samples in the dataset increases the slope of the confidence contours, reducing the spread of the distribution for a given mean. The plot on the far right shows the confidence contours for 10 survivors for the four failure doses of the 2N2222. The contours have a similar but more skewed shape to the contours derived only from the failure doses in Fig. 6, further constraining the parameter space.

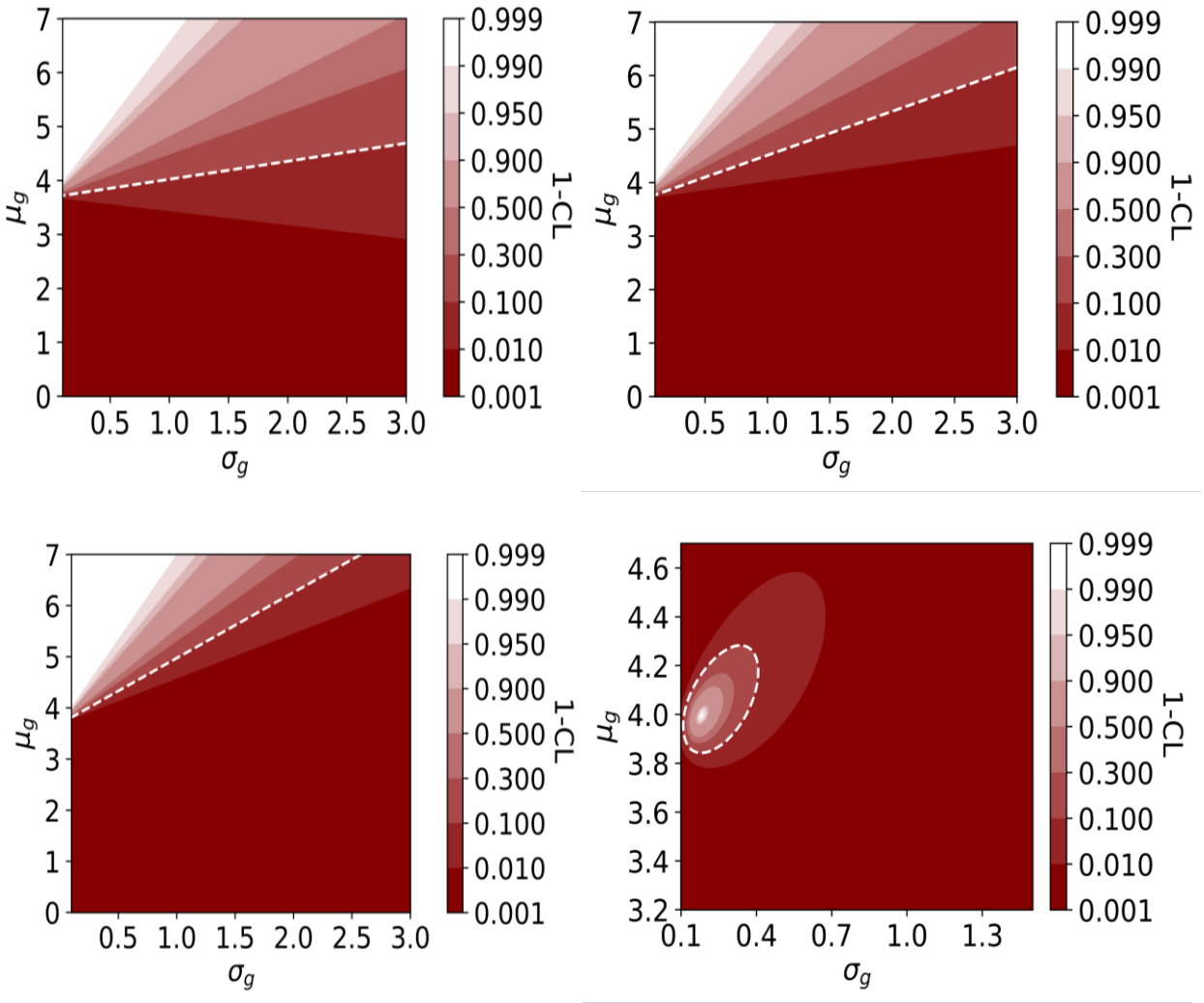

Fig. 7. Lognormal parameter space type-I censored likelihoods with datasets of 5, 10, and 22 survivors, tested to 40 krad(Si). The results of mixing 10 survivors with the 2N2222 failure doses are shown in the far-right image. The 90% confidence contour is emphasized with the white dashed line.

Unlike the cases where failure datapoints are included, the confidence boundary derived from survivors does not allow us to define a closed "area of interest" within the parameter space by itself. However, not all parameter space constitutes real, physical failure distributions expected for parts. For instance, when the standard deviation (or lognormal standard deviation) is extremely

large, the distribution is so wide that parts become as likely to fail at extremely low doses as at extremely high doses. This type of behavior is unusual for electronic parts; in fact, a lognormal standard deviation of about 0.5 has been selected as worst-case for silicon bipolar transistor failure distributions [38], [39]. Likewise, parts with mean failure doses in the Grad(Si) range are rare and typically unnecessary for space applications. To address this, engineering judgement is used to assess a realistic upper bound on expected device performance for the mission scenario. The upper dose to which a part is expected to survive is selected such that (a) the range of probable environment doses are orders of magnitude lower, and (b) the bounded P_{fail} is relatively insensitive to changes in upper dose. For this work, it is assumed that 99% of devices will fail by 1 Mrad(Si), so failure distributions describing device performance beyond this limit are not considered for $g(x)$. This limits the total parameter space searched and permits bounding of P_{fail} despite the lack of failure data. The largest P_{fail} within the 90% confidence level is defined as the metric for determining part suitability.

CHAPTER IV

DEMONSTRATION OF PROBABILISTIC FRAMEWORK

TID Example

The following paragraphs and figures are reprinted and modified from C. Champagne et al., "A confidence-based approach to including survivors in a probabilistic TID failure assessment," IEEE Trans. Nucl. Sci., Early Access, Nov. 2023. © 2023 IEEE.

To analyze the failure probability in the environment over the parameter space for device failure, each parameter pair is iterated over and used to generate the *g(x)* in (8), i.e., the device failure PDF. The failure probability within the environment is calculated with each parameter pair and plotted on a heat map. As a demonstration, one of the examples from Fig. 7 is used for a TID analysis, 10 survivors at 40 krad(Si). Similar cases are seen frequently in COTS datasets [40], [41], [42], [43].

The failure probabilities P_{fail} for the 2-year GEO, 200 mils Al shielding environment are shown in Fig. 8 over the parameter space of the lognormal *g(x)*. The 1-year environment is not shown but is similar. The 10-survivor data at 40 krad(Si) are used as an example for analysis within this environment. The 90% confidence contour of this 10-survivor sample is applied as a lower bound (line A). The upper dashed line in Fig. 8 (line B) represents the limit on expected part performance generated via engineering judgement. In summary, the P_{fail} contours are unique to the environment, dashed line A corresponds to the confidence contour derived from test data, and dashed line B corresponds to an upper bound on expected device performance.

By applying the 90% confidence contour and upper bound as a mask onto the P_{fail}, obtained by considering only the triangular area between the bounds, the failure probability of the device is bounded in the environment. The confidence contours for the mixed dataset can be applied as a

mask in similar fashion. The 5, 10, and 22 sample survivors in the 2-year environment yield worst-case failure probabilities of 8.6, 3.1, and 1.4%, respectively, to a 90% confidence level. The parameter pair for the worst-case device failure distribution for the 10-survivor example is shown by the dot at the intersection of the bounds in Fig. 8. Table II applies the procedure to TID test results on other parts found in the literature.

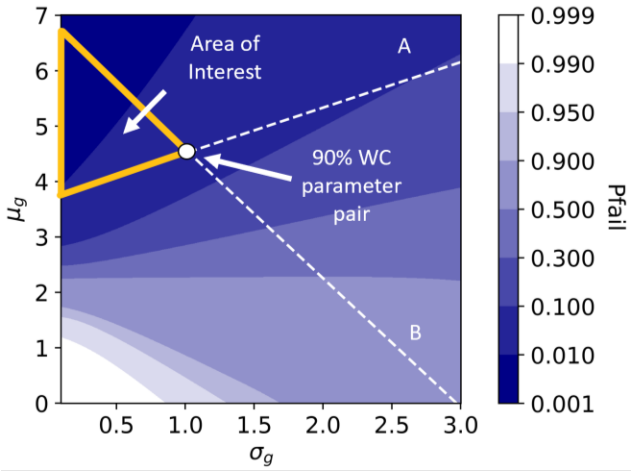

Fig. 8. Failure probabilities for a 2-year GEO, 200 mils Al shielding environment with the lower bound of the 90% confidence interval shown by the dashed line A, based on 10 survivors at 40 krad(Si). Line B forms an upper bound of realistic parameter pairs.

TABLE II
2 YEAR GEO, 200 MILS AL

Manufacturer Part Number	Test Results	WC P_{fail}, 90% CL (%)
Semicoa JANS2N2907AUB	88 survivors to 30 krad(Si) [41]	1.5
Semicoa JANS2N5339	10 survivors to 36 krad(Si) [41]	3.7
Microchip SY88422L	2 survivors to 100 krad(Si) [41]	10.0
Micropac 66212-301	12 survivors to 29.3 krad(Si) [41]	4.4
Maxim MAX913	5 survivors to 100 krad(Si) [42]	1.4
Semicoa JANSF2N2857	12 survivors to 300 krad(Si) [43]	1.0
Microchip MIC4427	1 failure at 20 krad(Si), 7 survived to 30 krad(Si) [44]	17.9

In addition to the environment analyzed in Fig. 8, other orbits and shielding thicknesses were analyzed for the lognormal device-failure parameter space. LEO and elliptical orbits showed similar failure probability contours to those in Fig. 8 but shifted along the μ_g axis (corresponding to increases and decreases in the mean total dose encountered), as did environments with different shielding thicknesses. The analysis for these environments remains the same. The resulting P_{fail} of a fixed *g(x)* and different environments are shown in Fig. 9. As the shielding thickness increases, the average dose encountered decreases, thus decreasing P_{fail}.

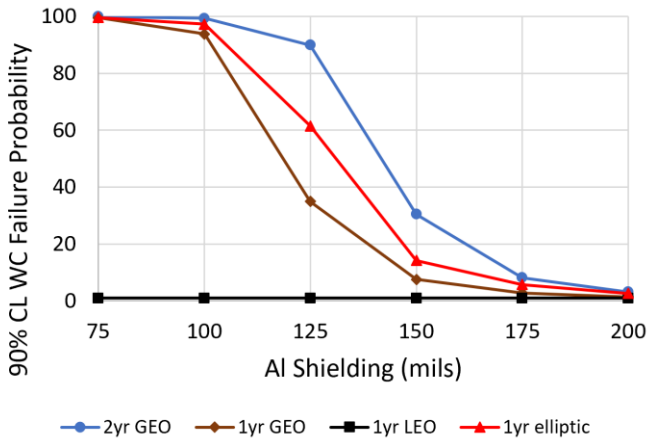

Fig. 9. The WC failure probability to a 90% CL of a device within different orbits with various thicknesses of Al shielding.

The effect of the upper bound, set at 99% device failure at 1 Mrad(Si), was investigated by modifying the total dose at which 99% of devices fail for the 10-survivor dataset. Halving the dose to 500 krad(Si) and doubling the dose to 2 Mrad(Si) only modified the 90% worst-case failure probability by roughly $\pm$1%, to 2.2% and 4.1%, respectively. These results indicate that the upper bound used to constrain the parameter space does not heavily influence the worst-case failure probability generated for this environment.

In addition to the lognormal distribution, the Weibull distribution is commonly used in cumulative failure analysis, including TID failure analysis [45], [46]. To ensure the analysis accommodates any type of distribution, the examples used previously were fit with Weibull curves instead of lognormal curves, and the environment P_{fail} space was mapped according to the Weibull shape and scale parameters. Since the two-parameter Weibull form was used, it has the same degree of freedom as the lognormal distribution. Thus, the relationship between the likelihood ratio and confidence level dictated by (10) remains the same. Fig. 10 shows the Weibull confidence contours for the same data used in the lognormal plots, with the scale parameter λ_g on the y-axis and the inverse shape parameter $1/k_g$ on the x-axis. The inverse shape parameter is plotted in order to be able to compare more readily with lognormal heatmaps, as the "area of interest" is unbounded for increasing k_g. However, as k_g increases, the failure probability decreases, so this does not affect our process of finding the worst-case failure probability.

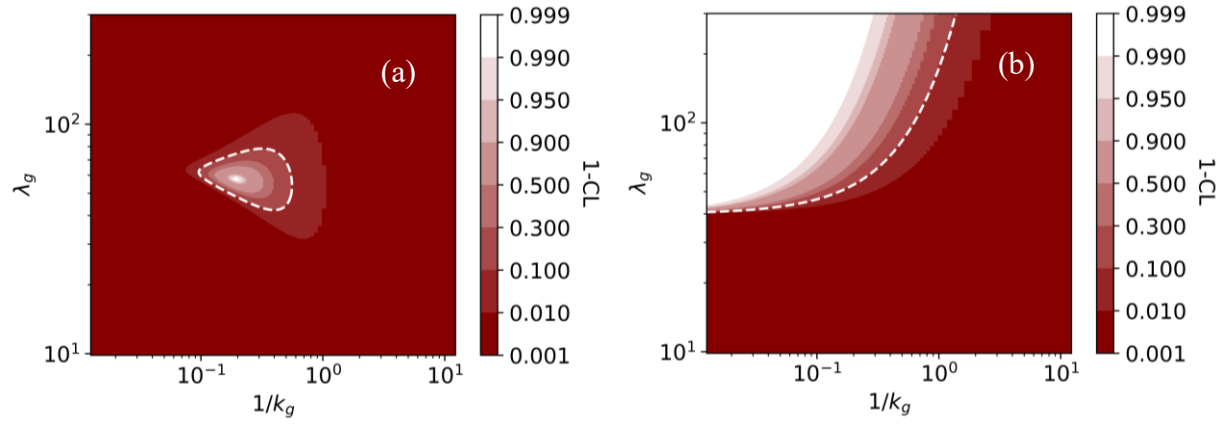

Fig. 10. Confidence contours for Weibull fits of the (a) 2N2222 failure doses and (b) 10 survivor, 40 krad(Si) data.

The failure probabilities for the GEO environment with a Weibull device failure distribution are shown in Fig. 11. The 90% worst-case failure probability parameter pair is indicated by the dot where the lower (line A) and upper (line B) bounds intersect. Both bounds were determined in the same way as the lognormal case. The 90% confidence level, worst-case failure probability for a Weibull fit of the data is 7.3%. Note that this P_{fail} is larger than that generated with a lognormal fit of the same data.

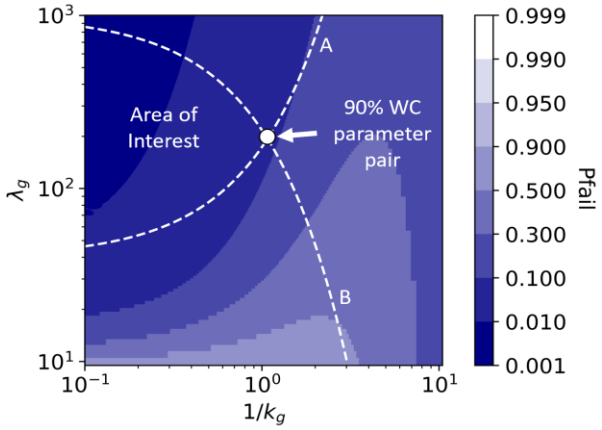

Fig. 11. Failure probabilities for the 2-year GEO environment mapped with a Weibull device failure distribution. Weibull scale and inverse shape parameters are along the y- and x-axis, respectively.

One should note that an additional restriction on the shape parameter, k_g, may also be necessary for proper modelling of the TID failure mechanism with Weibull. For k_g below 1, the Weibull function monotonically decreases rather than increasing to a peak and then decreasing. This type of function may be more representative of infant mortality than failure from cumulative effects.

Although the shape of the confidence and P_{fail} contours differ dramatically from the lognormal case, the contours still bound the worst-case P_{fail} within an area of interest, and the RHA

steps remain the same. As such, if there is uncertainty about the type of distribution that describes the device data, multiple different distributions may be examined. Other RHA methods may require an assumption of the device failure distribution [39].

The analysis presented so far has assumed the TID testing is performed *in-situ*; that is, device measurements are made while the device is being irradiated, allowing precise failure doses to be determined if failure is encountered. However, step-stress measurements may also be used for device characterization and lot testing [1], [47]. In many testing scenarios, step-stress may be the only practical test method. For instance, if a large number of devices must be read out, in-situ testing may prove too cumbersome. In this situation, device failures will be in dose bins rather than exact doses.

To extend the framework to incorporate interval data, the following likelihood formulation for readout data from [37] can be used,

$$\Lambda = C\left(\prod_{i=1}^{k}[F(T_i) - F(T_{i-1})]^{r_i}\right)[1 - F(T)]^{n-\sum_{i=1}^{k} r_i}. \quad (12)$$

Here Λ, C, F, and n are defined as in (10). (T_{i-1}, T_i) are the doses bounding the ith interval, with T_0 defined as 0. T is the dose to which the survivors were tested, k is the number of intervals, and r_i is the number of failure data points in the ith interval. Both survivor and failure data points are accounted for.

To elucidate this formulation with an example, consider the failure data for an AD9050 converter from [48], shown in Table III. Within a lower dose environment like a 1-year LEO orbit with 200 mils of Al shielding, the interval data produces a WC failure probability of 1.8% with 90% confidence. This method allows for a more rigorous examination of interval data than simply assuming failure at the starting dose of each bin, which may be overly conservative.

TABLE III
TID FAILURE FOR AD9050, IN INTERVALS

Dose Interval (in krad(Si))	Failures per Bin
0-5	1
5-10	2
10-20	0
20-30	3
30-50	1

Code Workflow

A workflow diagram for the code implementing the TID framework is shown in Fig. 12. The data from the environment model is fed into a Python script via a .csv file, where the first column is TID and the second column is cumulative probability. Doses are outputted into .txt files from IRENE, and a Python script is used to convert the .txt file to a .csv file. Doses are ranked smallest to largest (lowest percentile to highest percentile) and multiplied by two to achieve a full sphere of dose, as SHIELDOSE2 only outputs calculation over a hemisphere. Orbits over a time period of one year were simulated with environment models; for time periods longer than a year, doses were multiplied by the number of years desired. Once fed into the script, a linear interpolation is performed on the environment doses using the SciPy interp1d function.

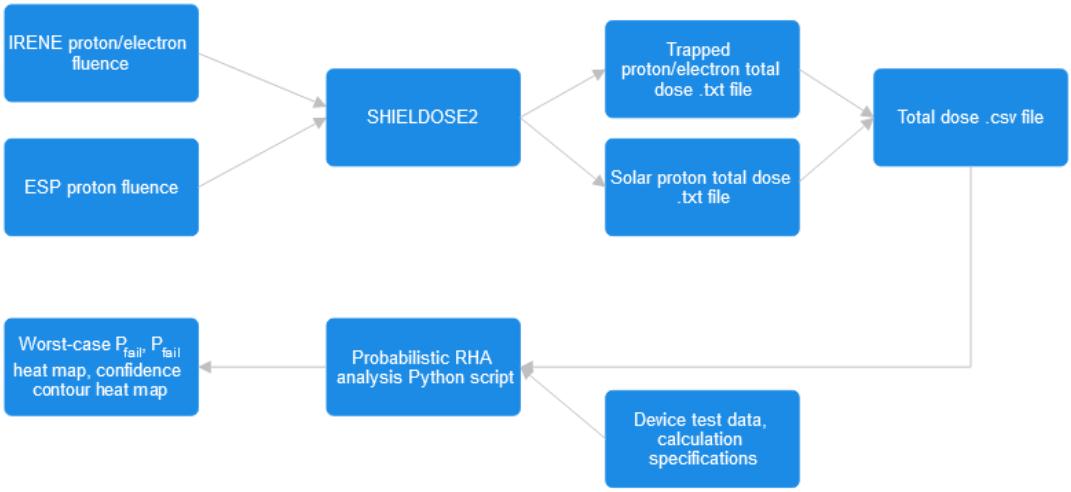

Fig. 12. Workflow diagram of the probabilistic TID RHA implementation.

One should note that, because a linear interpolation is used to create the environment CDF, the number of Monte Carlo trials used to generate the CDF will affect the resolution of the final P_{fail} calculation. In particular, the cumulative probability plateaus after the final inputted environment dose; for instance, if the largest simulated dose in the environment is 50 krad(Si) at the 99th percentile, then all doses above 50 krad(Si) will correspond to the 99th percentile also. Thus, the final P_{fail} will artificially plateau at 1% across the entire device parameter space. In order to achieve greater resolution sufficient for survivability requirements, additional trials from the environment models may be needed.

All other inputs, such as the device test data, parameter space area, parameter space upper bound, and P_{fail} calculation resolution, are specified in the Python script. If device failure data is being used, the failure doses are stored in a Python list object and the 'failures' mode is specified. If survivor data is used to bound P_{fail}, the dose survived to and the number of survivors are specified, as well as the 'survivors' mode. If both failures and survivors are being used to bound P_{fail}, the 'mixed' mode is specified.

The parameter space area over which calculations are performed is stored in a NumPy meshgrid object. Each coordinate in the meshgrid represents a parameter pair describing a device failure distribution PDF as a function of total dose. First, the likelihood of each PDF is evaluated using the input device test data to generate the parameter space likelihood-based confidence contours. Then, the failure probability is calculated with each PDF, and the confidence contours and upper bound are used to mask the unlikely or unrealistic of the parameter space. The index of the largest P_{fail} within the masked area is found and used as the worst-case distribution at the designated confidence level.

Displacement Damage Example

Displacement damage RHA follows the same general format as the TID RHA, the main difference being in the creation of the environment CDFs. Since DDD is in units of MeV/g and SHIELDOSE-2 only outputs rads, an alternative shield transport software was needed for transporting IRENE fluxes without the dose conversion. A local copy of the TRANS module in CREME96 [49] was used to transport all MC trials of proton fluxes in the orbit of the Hubble Space Telescope (HST) through 100 mils of aluminum shielding. The IRENE differential flux outputs were averaged over the year and divided by 4π to get in units of steradians. The TRANS module does not transport electrons, so only the trapped protons (AP9) were considered. Since protons are the dominant particle species for this orbit, neglecting the trapped electrons was deemed acceptable for this example. Further, solar protons are not expected to be a large contributor to displacement damage at this orbit, so ESP was not used for this example. After transporting the proton flux, the values were multiplied by a year (31,536,000 s) and 4π to get the omnidirectional differential fluence of each trial at each energy level. The fluence was then integrated with NIEL values for GaAs [50] as in (2) to achieve the DDD curve in Fig. 13.

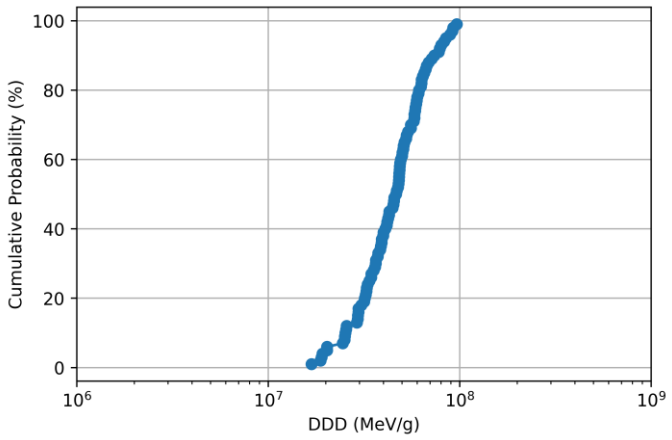

Fig. 13. The DDD curve due to trapped protons for the HST orbit with 100 mils of Al shielding over the course of a year.

From there, the framework for displacement damage assurance mirrors that for TID. If, for instance, one considers the ACPL-785E optocoupler [51] of which 10 survived to 1.49×10^{11} protons/cm^2 at 63 MeV, the NIEL value for that energy level can be calculated to generate the equivalent DDD tested to (5.82×10^{8} MeV/g). The analysis of this test data in the context of the 1-year HST orbit is shown in Fig. 14, and a worst-case failure probability of 1.03% is found. While the lognormal mean (μ_g) axis has shifted to higher values compared to TID, the P_{fail} heatmaps are otherwise very similar.

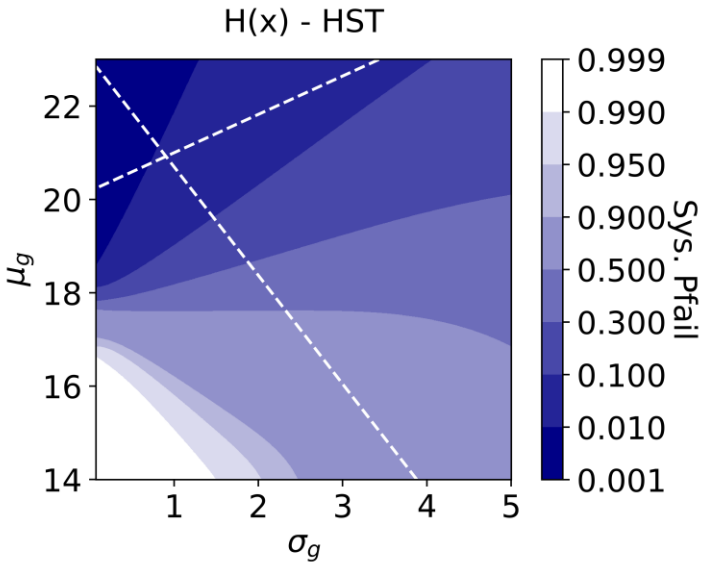

Fig. 14. The P_{fail} for the ACPL-785E optocoupler within the HST environment shown in Fig. 13.

CHAPTER V

The following paragraphs and figures are reprinted and modified from C. Champagne et al., "A confidence-based approach to including survivors in a probabilistic TID failure assessment," IEEE Trans. Nucl. Sci., Early Access, Nov. 2023. © 2023 IEEE.

APPLICATIONS

As mentioned previously and demonstrated in Table II, large databases of TID test data can be analyzed with this probabilistic framework to calculate worst-case failure probabilities for devices in a given environment. Beyond post-test analysis, the framework can be applied to test planning and heritage data applications to reduce testing costs and improve radiation testing efficiency.

Test Planning

When planning TID characterization or lot testing for devices, there are often constraints involving cost, beam time, availability of devices to test, etc. With regards to beam time, several factors may affect the degree of constraint inflicted on part testing. Test facility time slots can be expensive. Since TID is a cumulative effect, higher doses require longer test times unless dose rates are increased. However, dose rates often are constrained by available equipment and by requirements to match failure mechanisms in ground testing to those expected in use [9], [52]. This is a particular challenge for linear bipolar devices that are susceptible to ELDRS and require testing at low dose rates to match more closely those encountered in the space environment [10], [53].

Another common constraint experienced by test engineers is limited sample size. Especially if state-of-the-art or high-performance, individual parts may be expensive or in low supply, thereby limiting the number an engineer can test [21]. Additionally, each part represents

an additional test run at the radiation facility, increasing the beam time and engineering hours needed to complete testing.

The sample size and maximum total dose used for testing can be optimized for minimum cost or other constraints while meeting mission survival requirements within the probabilistic framework. Both testing parameters affect the confidence contours, thus dictating what a 90% confidence area of interest will be for a particular sample.

Fig. 15 demonstrates how the lower bound to the area of interest is affected by both the maximum total dose and the sample size. An increase in the maximum tested dose corresponds to an increase of the lower bound on the μ_g axis, corresponding to an increase in the estimated average failure dose. An increase in sample size increases the slope of the lower bound. In both cases, increasing the number of testing parameters, e.g., sample size and total dose level, compresses the area of interest and decreases the worst-case failure probability.

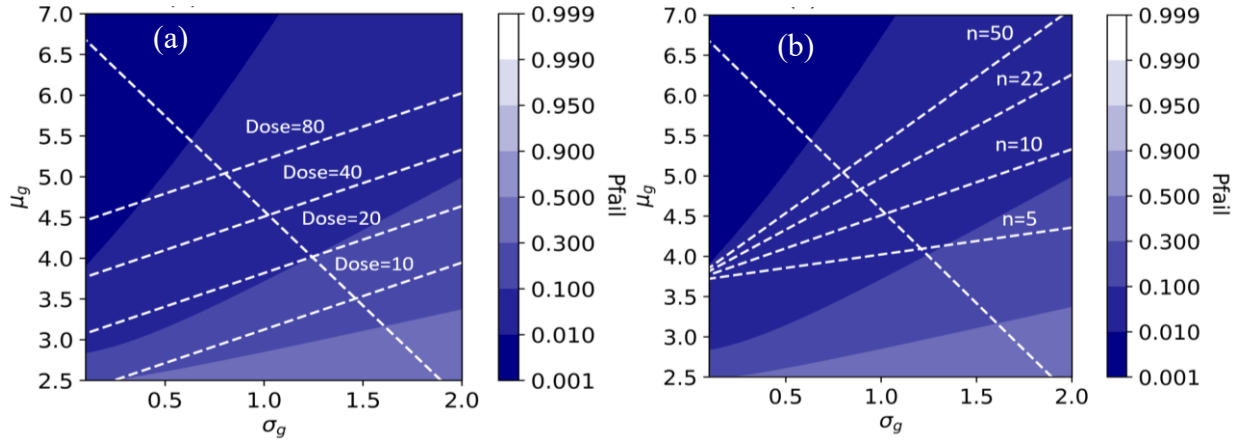

Fig. 15. Changes in the lower bound confidence contour by modifying (a) total dose and (b) sample size are shown within the context of the 2-year, 200 mils shielded GEO environment.

To find a relationship between sample size and tested dose for a particular survival requirement, the contour for the maximum allowable mission failure probability is analyzed in Fig. 16. Here a 1% maximum allowable P_{fail} is used. To ensure qualification if all devices survive testing, the area of interest should lie within the 1% failure probability contour. This provides two constraints: (1) where the 1% P_{fail} contour intersects the upper bound, and (2) where the 1% P_{fail} contour intersects the μ_g axis. By holding the device failure parameters constant at the values found at the first intersection, a relationship between sample size and tested dose can be found, as shown in Fig. 17. The second intersection relays a minimum overtest (regardless of sample size) that should be used when testing devices for the 2-year GEO, 200 mils shielding environment. This constraint is shown as the horizontal line in Fig. 17. For any pair of dose and sample size tested on or above both lines, if no failures occur during testing, the worst-case P_{fail} for the sample will be $\leq 1\%$ at a 90% confidence level, thereby meeting mission requirements. This relationship can be used to optimize a test for minimum cost or any other constraint.

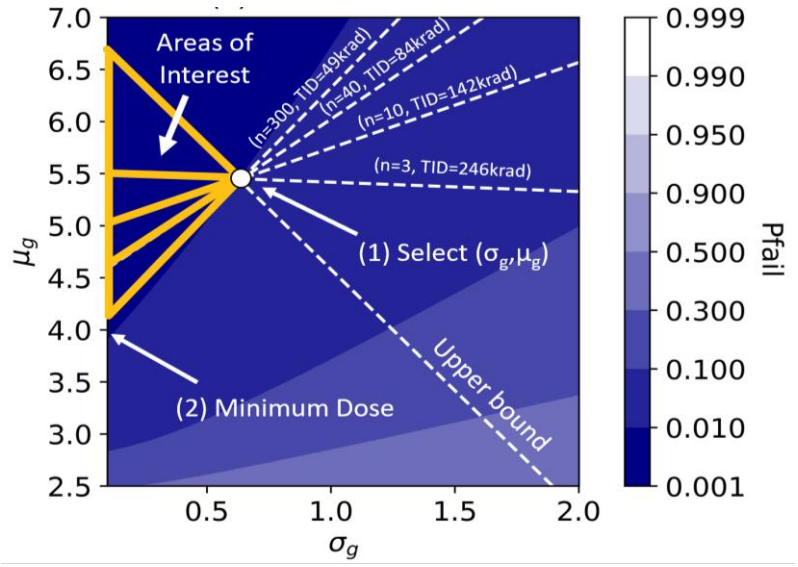

Fig. 16. A demonstration of how to use the failure probability contours to select a constant parameter set and overtest level for test planning. This example assumes an acceptable failure probability of 1%. Thus, the area of interest is forced to remain within this contour. The variables 'n' and 'TID' represent the sample size and maximum tested dose, respectively.

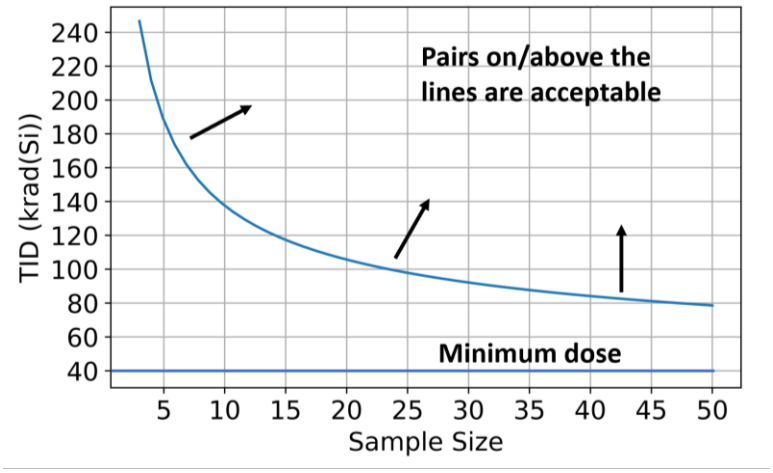

Fig. 17. Total dose-sample size pairs that produce a failure probability of 1% for a device failure distribution described by μ_g=5.45 and σ_g=0.64 in the 2-year GEO environment. Pairs on or above this curve and the minimum dose line will meet survival requirements if no failures are found during testing.

Heritage Data

Heritage data can further constrain the area of interest. This is done in [54] with RDM- and parameter-based TID RHA and can be incorporated into this framework. In the case where only a single device lot is available and the device operated successfully in a previous mission, heritage data can be treated as survivor data. The measured dose received on the mission acts as the maximum tested dose, and the steps for finding a worst-case failure probability are performed exactly as before.

Some important caveats should be kept in mind when using heritage data to qualify a part for a mission. If multiple lots of the device exist and the previously flown device is from a different lot, additional measures will need to be taken to account for lot-to-lot variability [55]. This is beyond the scope of this work. Additionally, care should be taken with the published dose in mission qualification documents. Exact doses from on-board dosimeters may be available, but if

precise measurements of mission dose are not recorded, an upper bound estimate on what the part experienced on-orbit is typically given in mission documentation. For hardness assurance, if a precise, measured dose is not available, a lower bound on dose must be used when analyzing heritage data. This may involve complex modeling of spacecraft shielding, where one usually assumes a lower dose generated by environment models to produce a sufficiently conservative lower bound.

CHAPTER VI

COMPARISON TO STANDARD RHA METHODS

The current military standards for conducting TID characterization and lot testing involve the use of the following hardness assurance methods: the radiation design margin (RDM), lot tolerance percent defective (LTPD) testing, and overtesting [1]. The new TID hardness assurance method presented in this thesis incorporates the variability of the space radiation environment over the course of a mission and a part's radiation response to calculate a metric for assessing part suitability. The incorporation of environment variability and mathematical rigor establishes greater confidence with fewer constraints than the other hardness assurance methods.

This chapter will compare the probabilistic TID hardness assurance framework with military hardness assurance standards to compare reliability metrics and use cases. All methods will be detailed, then an example dataset will be analyzed with the new framework and methods from the military standards. Justification for wide-spread adaptation of the new framework will be presented.

RDM

The standard method from [1] utilized by radiation test engineers is the RDM method. The RDM is defined as the ratio between a part's geometric mean failure dose, D_{fail}, and the expected mission environment dose, D_{env}, as shown in (13). Note that the geometric mean is used rather than the arithmetic mean because it is assumed that the part's failure behavior follows a lognormal distribution. If other distributions describe the part failure more accurately, the geometric mean may not be appropriate. An alternative metric utilizing critical parameter measurements – the parameter design margin, or PDM – is also commonly used. In this case, the ratio is between the

designated parametric failure value and the parametric degradation at the expected environment dose.

$$RDM = D_{fail}/D_{env} \tag{13}$$

The hardness of the part is categorized based on how large the RDM is, i.e., how far away the failure quantity is from the quantity expected during the mission. This categorization determines how often a part needs to be tested for usage in components of a mission (or multiple missions if in the same environment). The categories are HCC-1M (somewhat sensitive to TID), HCC-2 (less sensitive to TID), and HNC (insensitive to TID). Any part below the HCC-1M category is deemed unacceptable for usage in the environment. It should be noted that these categories are meant to serve as guidance to testing and procurement policies within a military context. An initial screening of parts resulting in an HNC categorization means that the part may be used without further screening. With an HCC-1M or HCC-2 categorization, parts may need to undergo additional testing as the mission(s) progress or as source control measures, ensuring that lot and part variability does not compromise the mission design [1]. These tests are described in the sections that follow.

In a method known as design margin breakpoint (DMBP), the RDM values which delineate the hardness categories are left to radiation effects engineers to define based on the requirements of their missions and engineering judgement. However, [1] does offer general guidelines based on historical use. The values given in Table IV date back to the Voyager missions [56] and are not based on rigorous mathematical analysis, but they are meant to be overly conservative and provide such large margins that the chance of TID-induced part failure is minimized.

Table IV. DMBP Method for Categorizing Piece Part Hardness

Category	Unacceptable	HCC-1M	HCC-2	HNC
RDM Range	RDM < 2 or 3	2 or 3 < RDM < 10	10 < RDM < 100	RDM > 100

The hardness categories may also be delineated using the part categorization criterion (PCC) method. This approach incorporates the spread of part radiation failure, the survival requirements, and the sample size of parts tested to determine the category breakpoints. Eq. 14 shows the PCC calculation, where K_{TL} is the one-sided tolerance limit [3] and s is the lognormal standard deviation of the part failure. Again, the part's failure distribution is assumed to be lognormal, hence usage of the lognormal standard deviation. This PCC value becomes the new breakpoint between classifications as shown in Table V. The PCC method is more statistical than DMBP and accounts for the spread of the test data, typically reducing the requirements for HCC-2 classification and the amount of required testing [1].

$$PCC = \exp\left(K_{TL}(P_s, CL, n) * s\right) \tag{14}$$

Table V. PCC Method for Categorizing Piece Part Hardness

Category	Unacceptable	HCC-1M	HCC-2	HNC
RDM Range	RDM < 2 or 3	2 or 3 < RDM < PCC	PCC < RDM < 100	RDM > 100

While usage of the PCC to delineate hardness classifications adds some mathematical rigor to the RDM method, an assumption of part failure distribution must be made, and many of the delineating values are still arbitrary. Additionally, usage of RDM may be overly conservative for certain applications, and there is no clear way to incorporate survival data at this step.

LTPD and Overtesting

Lot tolerance percent defective (LTPD) testing is one method employed for lot acceptance testing for parts falling into HCC-1M or HCC-2. In this scheme, binomial statistics are used to establish a required sample size with no failures so that lots with a set percentage of bad parts are rejected at a desired confidence level [1]. This method allows part analysis if the failure distribution is unknown [39]. A standard test is 11/0, 11 parts tested with no failures. At this sample size, a lot will be rejected if more than 20% of the constituent parts will fail at the environment dose at a 90% confidence level [1], [39]. A 22/0 test reduces the failure probability to 10% at a 90% confidence level. If the mission required the failure probability to be less than 1% at a 90% confidence level, a 230/0 test would be required.

To reduce the number of required parts tested to meet survival requirements, overtesting is employed, in which parts are tested to a dose level above the expected environment dose. A failure distribution must be known or assumed in order to quantify the overtest factor necessary to meet survival requirements, as well as a maximum standard deviation the distribution could have. There is no check on the effective sample size used during testing – the assumption of a maximized standard deviation is intended to make up for this, but this overtest method has been reported being overly conservative in rejecting lots and requiring high test doses [39]. As with RDM, both LTPD and overtest methods lack consideration of the variability of the environment.

Case Study

To see how the new probabilistic framework compares to the current hardness assurance standards, a CMOS analog switch from Maxim Integrated is considered. Analog switches select data paths for analog signals and are important components for many applications, such as multi-

channel data acquisition and instrumentation. Their small size, low power consumption, and fast switching times make them ideal for space applications [57]. In [58], 10 MAX4651 CMOS analog switches were irradiated with TID up to 100 krad(Si) without experiencing parametric failure. For the purposes of this case study, mission requirements are set at <1% failure probability at a 90% confidence level. A lognormal device failure distribution is also assumed as this distribution is commonly used in industry to describe piece part failure.

The environment of consideration is a 5-year, sun-synchronous orbit with perigee of 833 km, an apogee of 870 km, and an inclination of 98.594 degrees (the orbit of the NOAA 10 satellite [59]). The environment distribution is generated in AE9/AP9 [4] by ranking 199 Monte Carlo trials of total dose after 1 year in orbit, transporting through 100 mils of aluminum shielding, multiplying by 2 to achieve a full sphere, and multiplying by 5 to achieve a 5-year orbit, shown in Fig. 18.

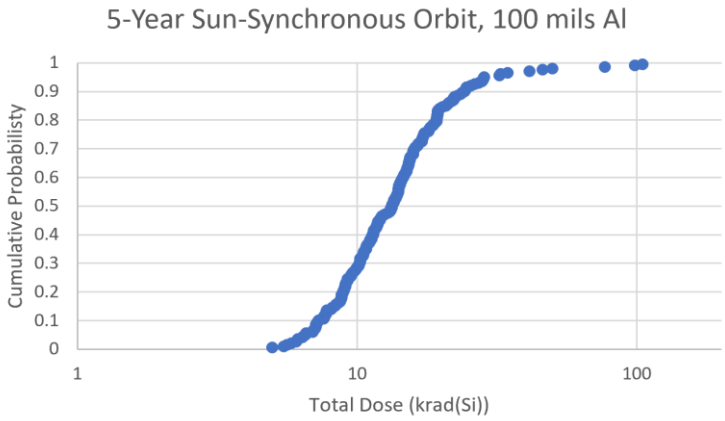

Fig. 18. Ranked Monte Carlo trials for a 5-year, sun-synchronous orbit, transported through 100 mils of Al shielding.

With current military standards, further testing of the part would need to be completed in order to qualify it for usage. With 1 as the maximum lognormal standard deviation, the 10/0 test, and the mission requirements of <1% failure at 90% confidence, the overtest factor equation from [39] yields 4.57 as the minimum overtest factor. The 90th percentile dose generated by AE9/AP9

for the environment under consideration is 24.3 krad(Si), so the analog switch should be tested to at least 111.1 krad(Si) in order for the part to satisfy requirements using this method. The analog switches have only been tested to 100 krad(Si), so further testing, an alternate part, or reassessment of engineering assumptions would be necessary to meet mission survival requirements.

However, using the probabilistic method, the environment doses from AP9/AE9 are ordered to form a cumulative distribution rather than taking the largest result. Assuming a lognormal distribution and an upper bound on the parameter space (99% failure at 1 Mrad(Si)), the lognormal parameter space can be analyzed within the context of the environment using (9) to generate a failure probability at the 90% confidence level. This method yields a failure probability of 0.826% to a 90% confidence level. These results satisfy mission requirements and enable part usage.

Discussion

There are multiple points during the standard overtest method in which choices affected the outcome of the part qualification. For instance, the part failure distribution was assumed to be a well-behaved lognormal distribution, and the maximum lognormal standard deviation for part failure distribution was assumed to be 1. A choice of a smaller maximum would have reduced the required overtest for the part. This choice may be made with additional analysis of similar parts to the analog switch under consideration [38]; however, this also introduces ambiguity regarding which parts qualify as “similar” to the part in question. Must the similar parts be of the same manufacturer? Or should they be of the same technology generation, but various manufacturers may be considered? Can any CMOS technology be classified as “similar”? Especially when dealing with COTS parts, the answers may be ambiguous as variability under irradiation may be

larger than controlled parts. These choices are left to the radiation effects engineer to decide and justify.

Additionally, the 90th percentile total dose generated by AE9/AP9 was chosen as the environment spec dose. Most military hardness assurance practices stem from a risk-avoidance stance, so worst-case constants and overdesign are incorporated into hardness assurance. Engineers may elect to choose a smaller or larger percentile dose to use in the overtest analysis, which may reduce or increase the overtest margin required significantly. However, as above, this choice is left to the radiation effects engineer to justify and can be a somewhat arbitrary choice based on the risk posture of the mission.

For the probabilistic method, a couple of assumptions were made as well, the biggest one being that the part failure distribution is a well-behaved lognormal distribution (also made with the overtest method above). An assumption on the upper bound of the parameter space was also made, however, this assumption has some justification (see Chapter 3).

While the case study discussed above demonstrates how the probabilistic analysis may be less conservative than traditional hardness assurance methods in some instances, there are other instances where the probabilistic method turned out to be just as conservative, if not more so, than traditional methods. Fig. 19 shows (1) overtest factors calculated with the traditional overtest method of [39] with a maximum lognormal standard deviation of 1 and 0.5 assumed, and (2) overtest factors calculated with the probabilistic method for the sun-synchronous environment using the test planning steps outlined in Chapter 5. If the maximum σ_g is 1, the overtest method from [39] is more conservative than the probabilistic method for sample sizes less than or equal to 15. Beyond this point, because of the lack of environment variability consideration, the traditional method overtest factor continues decreasing and becomes less conservative than the probabilistic

method. If the maximum σ_g is 0.5, the probabilistic method is more conservative regardless of sample size.

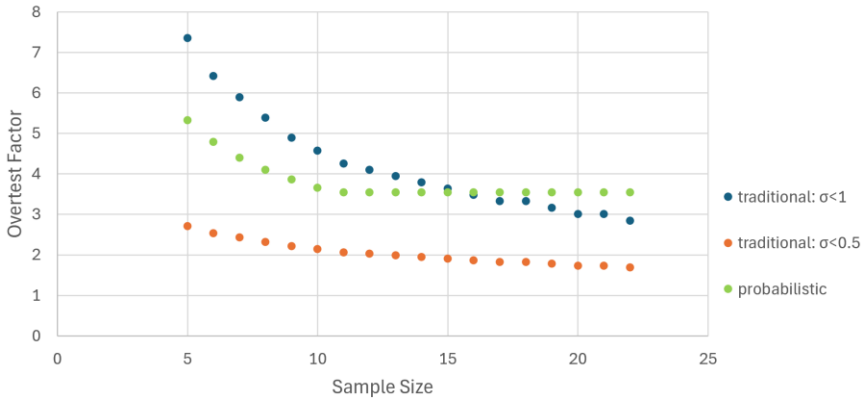

Fig. 19. Overtest factors calculated using the approach from [39] and the probabilistic method for the 5-year sun-synchronous orbit. A 1% failure probability to a 90% confidence level is used for the overtest calculation.

Overall, the probabilistic method involves less engineering judgement calls which may or may not be arbitrary. The method is mathematically rigorous and incorporates both environment and device behavior variability, producing a metric for part qualification that is grounded in part operation within the environment.

CHAPTER VII

CONCLUSIONS

This work expands on a probabilistic TID RHA framework by enabling the use of survivor data to bound the device failure probability in a user-specified environment. By using the type-I likelihood equation to calculate confidence contours, a lower bound is placed on the parameter space. An upper bound on physical device failure distributions is used to further constrain the parameter space and calculate a worst-case P_{fail} at the 90% confidence level. Any environment or device failure fit can be analyzed, and both in-situ and interval tests can feed the device failure model. Both TID and DD examples were worked through with the framework. The framework can be used for test planning purposes, optimizing tested dose and sample size for cost or any other testing constraint. Costs may be further reduced with heritage data, which can be treated as survivors when devices of the same lot have successfully flown in previous missions. However, obstacles and limits exist on the amount of constraint heritage data can impose on P_{fail}, namely from the estimated dose received on the mission.

Unlike established hardness assurance methods, the probabilistic framework accounts for the variability from both the space environment and the part behavior under irradiation. Established methods stem from postures of risk-avoidance, resulting in margins which may be more or less conservative than intended and ambiguity when using engineering judgement to relax constraints. Less assumptions are required to use the probabilistic method, and there is more justification for the assumptions made. As such, existing part data may be used to quantify part risk and qualify usage of more parts with the new method, potentially reducing hardness assurance constraints. The novel framework allows an engineer to consider all available TID data on a

candidate device, resulting in a quantitative assessment of survival in a variable space environment.

The preceding paragraphs are reprinted and modified from C. Champagne et al., "A confidence-based approach to including survivors in a probabilistic TID failure assessment," IEEE Trans. Nucl. Sci., Early Access, Nov. 2023. © 2023 IEEE.

REFERENCES

[1] *Ionizing Dose and Neutron Hardness Assurance Guidelines for Microcircuits and Semiconductor Devices*, MIL-HDBK-814, Department of Defense, 1994.

[2] M. A. Xapsos *et al.*, "Inclusion of radiation environment variability in total dose hardness assurance methodology," *IEEE Trans. Nucl. Sci.*, vol. 64, no. 1, pp. 325–331, Jan. 2017.

[3] R. Ladbury and T. Carstens, "Development of TID hardness assurance methodologies to capitalize on statistical radiation environment models," *IEEE Trans. Nucl. Sci.*, vol. 68, no. 8, pp. 1736–1745, Aug. 2021.

[4] G. P. Ginet *et al.*, "AE9, AP9 and SPM: New models for specifying the trapped energetic particle and space plasma environment," *Space Sci. Rev.*, vol. 179, no. 1–4, pp. 579–615, Dec. 2013.

[5] M. A. Xapsos and G. P. Summers, "Probability model for cumulative solar proton event fluences," *IEEE Trans. Nucl. Sci.*, vol. 47, no. 3, pp. 486–490, Jun. 2000.

[6] P. Jiggens *et al.*, "The solar accumulated and peak proton and heavy ion radiation environment (SAPPHIRE) model," *IEEE Trans. Nucl. Sci.*, vol. 65, no. 2, pp. 698–711, Feb. 2018.

[7] Z. D. Robinson *et al.*, "Mission specific solar radiation environment model (MSSREM): Peak flux model," *Space Weather*, vol. 18, no. 8, Aug. 2020, Art. no. 2019SW002361.

[8] J. R. Schwank *et al.*, "Radiation effects in MOS oxides," *IEEE Trans. Nucl. Sci.*, vol. 55, no. 4, pp. 1833–1853, Aug. 2008.

[9] D. M. Fleetwood and H. A. Eisen, "Total-dose radiation hardness assurance," *IEEE Trans. Nucl. Sci.*, vol. 50, no. 3, pp. 552–564, Jun. 2003.

[10] D. M. Fleetwood, “Total ionizing dose effects in MOS and low-dose-rate-sensitive linear-bipolar devices,” *IEEE Trans. Nucl. Sci.*, vol. 60, no. 3, pp. 1706–1730, Jun. 2013.

[11] J. R. Srour, C. J. Marshall, and P. W. Marshall, “Review of displacement damage effects in silicon devices,” *IEEE Trans. Nucl. Sci.*, vol. 50, no. 3, pp. 653–670, Jun. 2003.

[12] J. R. Srour, “Displacement damage effects in electronic materials, devices, and integrated circuits,” in *Notes from the 1988 IEEE Nuclear and Space Radiation Effects Short Course*, Portland, OR.

[13] A. H. Johnston, “Radiation effects in optoelectronic devices,” *IEEE Trans. Nucl. Sci.*, vol. 60, no. 3, pp. 2054–2073, Jun. 2013.

[14] R. A. Reed *et al.*, “Emerging optocoupler issues with energetic particle-induced transients and permanent radiation degradation,” *IEEE Trans. Nucl. Sci.*, vol. 45, no. 6, Dec. 1998.

[15] J. Lloyd. (2018). “Statistics and physics in reliability. You can’t have one without the other” [PowerPoint slides]. Available: https://nepp.nasa.gov/docs/etw/2018/19JUNE18/1330b%20-%20LLoyd%20-%20Statistics%20and%20Physics%20in%20Reliability%20(2).pdf

[16] “1.3.6.6.9. Lognormal distribution.” NIST/SEMATECH e-Handbook of Statistical Methods. Available: https://www.itl.nist.gov/div898/handbook/eda/section3/eda3669.htm (accessed Feb. 14, 2024).

[17] J. Chen and A. M. Korsunsky, “Why is local stress statistics normal, and strain lognormal?,” *Mater. Des.*, vol. 198, Jan. 2021, Art. no. 109319.

[18] C. Furusawa *et al.*, “Ubiquity of log-normal distributions in intra-cellular reaction dynamics,” *Biophysics*, vol. 1, pp. 25–31, Feb. 2005.

[19] P. J. McWhorter, S. L. Miller, and W. M. Miller, “Modeling the anneal of radiation-induced trapped holes in a varying thermal environment,” *IEEE Trans. Nucl. Sci.*, vol. 37, no. 6, Dec. 1990.

[20] P. S. Winokur *et al.*, “Correlating the radiation response of MOS capacitors and transistors,” *IEEE Trans. Nucl. Sci.*, vol. NS-31, no. 6, Dec. 1984.

[21] K.A. LaBel *et al.*, “Emerging radiation hardness assurance (RHA) issues: A NASA approach for space flight programs,” *IEEE Trans. Nucl. Sci.*, vol. 45, no. 6, pp. 2727-2736, Dec. 1998.

[22] M. R. Shaneyfelt *et al.*, “Hardness variability in commercial technologies,” *IEEE Trans. Nucl. Sci.*, vol. 41, no. 6, pp. 2536–2543, Dec. 1994.

[23] A. I. Namenson, “Lot uniformity and small sample sizes in hardness assurance,” *IEEE Trans. Nucl. Sci.*, vol. 35, no. 6, pp. 1506–1511, Dec. 1988.

[24] Q. Zheng *et al.*, “Measurement and evaluation of the within-wafer TID response variability on BOX layer of SOI technology,” *IEEE Trans. Nucl. Sci.*, vol. 68, no. 10, pp. 2516–2523, Oct. 2021.

[25] Y. Li *et al.*, “Including the effects of process-related variability on radiation response in advanced foundry process design kits,” *IEEE Trans. Nucl. Sci.*, vol. 57, no. 6, pp. 3570–3574, Dec. 2010.

[26] C. M. Mezzomo *et al.*, “Characterization and modeling of transistor variability in advanced CMOS technologies,” *IEEE Trans. Electron Devices*, vol. 58, no. 8, pp. 2235–2248, Aug. 2011.

[27] “AP8MIN and AP8MAX trapped proton models.” CRÈME-MC Site. Available: https://creme.isde.vanderbilt.edu/CREME-MC/help/ap8min-and-ap8max-trapped-proton-models (accessed Dec. 28, 2023).

[28] “Background: Trapped particle radiation models.” The Space Environment Information System (SPENVIS). Available: https://www.spenvis.oma.be/help/background/traprad/traprad.html (accessed Dec. 28, 2023).

[29] “IRENE-AE9/AP9/SPM Home.” Virtual Distributed Laboratory (VDL), U.S. Air Force. Available: https://www.vdl.afrl.af.mil/programs/ae9ap9/index.php (accessed Feb. 08, 2024).

[30] “IRENE-AE9/AP9/SPM Downloads.” Virtual Distributed Laboratory (VDL), U.S. Air Force. Available: https://www.vdl.afrl.af.mil/programs/ae9ap9/downloads.php (accessed Dec. 28, 2023).

[31] “Emission of Solar Protons (ESP) Model (MFS-31315-1).” NASA Technology Transfer Program. Available: https://software.nasa.gov/software/MFS-31315-1 (accessed Dec. 28, 2023).

[32] “SPENVIS - Space Environment, Effects, and Education System.” The Space Environment Information System (SPENVIS). Available: https://www.spenvis.oma.be/ (accessed Jan. 04, 2024).

[33] M. White and J. B. Bernstein, “Microelectronics reliability: Physics-of-failure based modeling and lifetime evaluation,” *JPL/Cal. Inst. Tech.*, Feb. 2008, Art. no. 08-5.

[34] D. Kerwin, “Reliability and qualification of custom integrated circuits for harsh environment applications using commercial wafer foundries qualification,” in *Notes from the 2010 IEEE Nuclear and Space Radiation Effects Short Course*, Denver, CO.

[35] E. A. Amerasekera and F. N. Najm, *Failure Mechanisms in Semiconductor Devices*, 2nd ed. West Sussex: John Wiley & Sons Ltd, 1997.

[36] Y. Pawitan, *In All Likelihood: Statistical Modelling and Inference Using Likelihood*. Oxford, U.K.: Oxford Univ. Press, 2001.

[37] "8.4.1.2. Maximum likelihood estimation." NIST/SEMATECH e-Handbook of Statistical Methods. https://www.itl.nist.gov/div898/handbook/apr/section4/apr412.htm (accessed Mar. 21, 2023)

[38] A. I. Namenson, "Statistical treatment of damage factors for semiconductor devices," *IEEE Trans. Nucl. Sci.*, vol. 26, no. 5, pp. 4691–4694, Oct. 1979.

[39] A. I. Namenson, "Hardness assurance and overtesting," *IEEE Trans. Nucl. Sci.*, vol. 29, no. 6, pp. 1821–1826, Dec. 1982.

[40] S. Zajac *et al.*, "Extended compendium of total ionizing dose (TID) test results for the Europa Clipper mission," in *2022 IEEE Radiation Effects Data Workshop*, Provo, UT, pp. 28-41.

[41] A. D. Topper *et al.*, "NASA Goddard Space Flight Center's recent radiation effects test results," in *2022 IEEE Radiation Effects Data Workshop*, Provo, UT, pp. 117-123.

[42] A. N. Bozovich and F. Irom, "Compendium of single event transient (SET) and total ionizing dose (TID) test results for commonly used voltage comparators," in *2017 IEEE Radiation Effects Data Workshop*, New Orleans, LA, pp. 16-36.

[43] A. N. Bozovich *et al.*, "Compendium of total ionizing dose (TID) test results for the Europa Clipper mission," in *2018 IEEE Radiation Effects Data Workshop*, Waikoloa, HI, pp. 28-38.

[44] A. Topper and M. Casey, "MIC4427 MOSFET driver total ionizing dose test report," SSAI/NASA GSFC, Greenbelt, MD, USA, Mar. 2020.

[45] W. Weibull, "A statistical distribution function of wide applicability," *J. Appl. Mech.*, vol. 18, no. 3, pp. 293–297, Sep. 1951.

[46] S. Libertino *et al.*, "Ionizing radiation effects on nonvolatile read only memory cells," *IEEE Trans. Nucl. Sci.*, vol. 59, no. 6, pp. 3016–3020, Dec. 2012.

[47] A. I. Namenson, “Statistical analysis of step stress measurements in hardness assurance,” *IEEE Trans. Nucl. Sci.*, vol. 31, no. 6, pp. 1398–1401, Dec. 1984.

[48] A. K. Sharma, K. Sahu, and S. Kniffin, “Evaluation of high performance converters under low dose rate total ionizing dose (TID) testing for NASA programs,” in *1998 IEEE Radiation Effects Data Workshop*, Newport Beach, CA, pp. 142-147.

[49] “Welcome to the CRÈME site” CRÈME-MC Site. Available: https://creme.isde.vanderbilt.edu/CREME-MC (accessed Feb. 11, 2024).

[50] “Protons & Ions NIEL Dose Calculator.” SR-NIEL-7 Calculator. Available: https://www.sr-niel.org/index.php/sr-niel-web-calculators/niel-dose-calculator-for-spectral-fluence-of-electrons-protons-and-ions/protons-ions-niel-dose-calculator (accessed Feb. 12, 2024).

[51] A. D. Topper *et al.*, “NASA Goddard Space Flight Center's compendium of recent total ionizing dose and displacement damage dose results,” in *2018 IEEE Radiation Effects Data Workshop*, Waikoloa, HI.

[52] P. S. Winokur *et al.*, “Total-dose radiation and annealing studies: Implications for hardness assurance testing,” *IEEE Trans. Nucl. Sci.*, vol. 33, no. 6, pp. 1343-1351, Dec. 1986.

[53] R. L. Pease, R. D. Schrimpf, and D. M. Fleetwood, “ELDRS in bipolar linear circuits: A review,” *IEEE Trans. Nucl. Sci.*, vol. 56, no. 4, pp. 1894–1908, Aug. 2009.

[54] R. Ladbury and B. Triggs, “A Bayesian approach for total ionizing dose hardness assurance,” *IEEE Trans. Nucl. Sci.*, vol. 58, no. 6, pp. 3004–3010, Dec. 2011.

[55] R.L. Pease, “Total dose issues for microelectronics in space systems,” *IEEE Trans. Nucl. Sci.*, vol 43, no. 2, pp. 442-455, Apr. 1996.

[56] “Radiation design margin requirement.” NASA.gov. https://llis.nasa.gov/lesson/792 (accessed Sep. 19, 2023).

[57] “Analog switches and multiplexers basics,” Analog Devices, Rep. *MT-088*, 2009.

[58] J. Osheroff and T. Wilcox, “Total Ionizing Dose Test Report MAX4651 Quad SPST Analog Switch,” NASA GSFC, Greenbelt, MD, USA, April 2021.

[59] “NOAA 10.” NASA Space Science Data Coordinated Archive. https://nssdc.gsfc.nasa.gov/nmc/spacecraft/displayTrajectory.action?id=1986-073A (accessed Feb. 27, 2024).